CDF Note No. 355
February 24, 1986

MEASUREMENTS OF DRIFT VELOCITIES AND LORENTZ ANGLES AT 15KG

M. Atac, E. Coleman, T. Hessing, R. W. Kadel, M. Pratt and R. L. Wagner
Fermi National Accelerator Laboratory, P.O. Box 500
Batavia, Illinois 60510

ABSTRACT

We have measured the drift velocities and Lorentz angles of electrons in several candidate gases for the CDF Central Tracking Chamber at magnetic fields of 10kG, 13.5kG, and 15kG. The gases include argon/ethane(50/50), argon/ethane/ethyl-alcohol mixtures, and argon/CO_2/methane(89/10/1). For the preferred gas mixture of argon/ethane(50/50) bubbled through alcohol at -7.2°C, we studied the sensitivity of the drift velocities and Lorentz angles to changes in electric field, magnetic field, alcohol temperature, and argon/ethane ratio. Measurements with argon/methane(80/20) at 5kG and 10kG are also presented.

1) INTRODUCTION

The Central Tracking Chamber (CTC) of the Colliding Detector at Fermilab (CDF) will operate with the drift electric field perpendicular to a 15kG magnetic field and therefore must deal with a large angle of electron drift with respect to the direction of the electric field. At small electric fields, this Lorentz angle is predicted to follow

Eq. 1 $$\tan(\eta) = (v_0 B)/(E),$$

where E is the electric field, η is the Lorentz angle, B is the magnetic field perpendicular to the electric field, and $v_0 = v(E,B=0)$ is the drift

velocity at B=0. Unfortunately, Eq. 1 breaks down far below electric field values that are required to operate the CTC, and the predictions for high electric fields are uncertain.

The 3.21m long sense and field shaping wires of the CTC run along the beam direction parallel to the solenoidal magnetic field. The 6156 sense wires are divided along the radial direction from the beam line into 9 "super layers" as shown in Figure 1. The layers alternate between wires in the axial or beam direction and wires at a ±3° stereo angle with respect to the beam direction. The stereo scheme of measuring position along the beam direction was chosen over charge division for its comparative ease of readout and better resolution. With the super layer design, there are a number of advantages in tilting "super cells" (see Figure 2) within the super layers to compensate for the large Lorentz angle at 15kG: 1) Electron drift in the ϕ direction optimizes the sampling frequency by minimizing dead regions at the super layer borders. 2) By design, a high transverse momentum (p_T) track must cross the sense wire plane in each layer it traverses. This simplifies online triggering with high p_T tracks in the central region and provides a means to separate very closely spaced (<1mm) tracks in jets. 3) The left/right ambiguity is easily resolved because the ghost track defined by the improper assignment is rotated with respect to the true track direction by ~70°. 4) Drift in the ϕ direction minimizes sensitivity of the position resolution to fluctuations in the Lorentz angle for high p_T tracks, which travel approximately in the radial direction.

The choice of a 45° tilt angle was based on these considerations and previous measurements[1] with argon/ethane(50/50) [AR/ET(50/50)] at 15kG. Since operation with pure AR/ET(50/50) can result in polymerization on chamber wires, we hope to operate the CTC with this mixture bubbled through

ethyl alcohol at approximately -7°C which has been shown[2] to inhibit polymerization. Studies with prototype chambers at B=0 indicate that the addition of alcohol at -7°C does not significantly effect the position resolution or produce excessive electron attachment at the CTC's maxixmum drift distance of 3.5cm. The main purpose of this experiment was to determine the CTC's operating electric field and drift velocity at 15kG for AR/ET(50/50) bubbled through ethyl alcohol at -7.2°C (our "preferred gas"). Operating points were measured for other candidate gases including pure AR/ET(50/50), AR/CO_2/METHANE(89/10/1), and AR/ET(40/60). For the preferred gas, the sensitivities of v and tan(η) to variations in the argon/ethane ratio, alcohol temperature, magnetic field, and electric field were studied. Measurements were also made at 5kG and 10kG with AR/METHANE(80/20), a gas that will be used by the Vertex Time Projection Chamber (VTPC) in CDF.

2) THE EXPERIMENT

2.1) OVERVIEW OF THE APPARATUS AND EXPERIMENTAL PROCEDURE

The experiment was performed in the CDF Assembly Hall at Fermilab using a BM106 dipole magnet. A schematic of the apparatus is shown in Figure 3, and the measurement scheme and data acquisition are illustrated in Figure 4. A 2.0mCi ^{90}Sr beta source was glued to the bottom pole face of the magnet and provided a beam of electrons for ionizing gas molecules in the drift chamber. A signal from a Hamamatsu silicon photodiode glued to the top pole face indicated the arrival of an electron from the source which had passed through the chamber in a direction parallel to the magnetic field. The source was collimated by a 2mm diameter hole in a 19.1mm thick

lead disk, and the photodiode was collimated by a 3.18mm diameter hole in a 9.43mm thick lead disk.

As illustrated in Figure 4, the drift chamber consisted of a region of uniform electric field that was separated from the anode wire and cathode pads by a wire grid. The chamber was positioned so that electrons from the source traversed a known location in the uniform field region. The time difference between the anode and photodiode signals indicated the drift time of electrons from the point of ionization by the source electron to the anode wire. The anode signal also gated an ADC unit which integrated the charge on each of 8 pads that surrounded the point of arrival on the anode wire. The centroid of pad charges gave the x-position of the arriving electrons.

In order to eliminate the effects of electric field non-uniformity near the readout portion of the chamber, v and tan(η) were calculated from differences between measurements at "NEAR" and "FAR" y-positions in the uniform field region as shown in Figure 4. For each reading the chamber was moved in x to give the same "nominal" pad centroid value within ±0.4mm. The small differences from the nominal value were corrected by the pad centroid readings, and the velocity and Lorentz angle were then found from

Eqs. 2 $\tan(\eta)=\Delta x/\Delta y$ and $v=(\Delta x^2+\Delta y^2)^{1/2}/\Delta TDC$,

where Δ indicates the difference between the NEAR and FAR values and TDC refers to the time differnce between the anode and photodiode signals.

2.2) DRIFT CHAMBER

An elevation view of the drift chamber is shown in Figure 5a. The uniform electric field was created by 125μm diameter gold plated Be-Cu wires wound with a 2mm pitch. These field shaping wires were cut between winds

and connected by 22MΩ resistors. A negative high voltage was applied to a wire 77.8mm from the grid, and the grid and the field wire nearest the grid (76mm from the first wire) were connected to ground. The FAR and NEAR y-positions of the source were 13mm from the high voltage connection and from the grid, respectively. The grid was made from 100μm diameter Cu wires spaced by 1mm. The anode was a 25μm diameter gold plated tungsten wire and was normally operated at +2050v. The 7mm wide pads surrounded the anode wire on three sides and were constructed from copper-clad DuPont G-10 fiberglass. The anode and pad signals were amplified at the chamber by Centralab IO354 hybrid preamplifiers and subsequently by another factor of 10 by the LRS612 NIM module.

The electric field was calculated using a computer program that was originated by J. Va´Vra at SLAC. For HV=-9.5kV, the calculated equipotential lines are shown in Figure 5a, and the calculated electric field is shown as a function of the y-coordinate in Figure 5b. The electric field was within 0.5% of the central maximum value over 70% of the drift region between the NEAR and FAR locations and fell to 2% below the central value at the two extremes. The electric fields listed in the data tables are the average values between the NEAR and FAR locations. The quantities v and tan(η) were calculated assuming a constant electric field between the NEAR and FAR positions, but the errors introduced by this approximation were negligible compared to other experimental errors. During the measurements the negative high voltage ranged from 3.8kV to 13.3kV which corresponded to electric fields of 0.492kV/cm and 1.722kV/cm. The calibration of the Bertan 205A-20N power supply was checked by the Fluke 8840A precision resistor divider up to 6kV, and the two devices agreed to better than 0.15%. From this measurement and the precision of the chamber construction we estimate

the absolute error in the electric field to be 1% and the differences in field between points in the chamber separated by 100mm in x to be less than 0.5%

2.3) CHAMBER POSITIONING DEVICE AND ALIGNMENT CORRECTIONS

As shown in Figure 3, the chamber was firmly mounted on an aluminum plate which rolled on teflon balls atop a long u-channel. The y-position of the chamber relative to the source (NEAR or FAR) was determined by a pair of dowel pins that fit into one or the other of two sets of holes in the chamber mounting plate. The reproducibility of the chamber position in the y-coordinate was 25μm, and is negligible compared to the 50.8mm separation of the NEAR and FAR locations.

The chamber's x-position was remotely adjusted by a precision screw slide which was attached to the channel outside the magnetic field. Motion was induced by a stepping motor and measured by dial indicators to an accuracy of <10μm. This error was negligible compared to that of the pad centroid measurement.

Chamber misalignments could occur if movement of the chamber in the y-coordinate was not parallel to $\vec{E}$ or if movement of the chamber in the x-coordinate was not perpendicular to $\vec{E}$. We measured these misalignments with the source and chamber at B=0 and made appropriate corrections to v and tan(η). The misalignment in plate movement caused an x-offset of 0.082±0.070mm between the NEAR and FAR positions, and the channel movement was aligned to within 0.057° with respect to the perpendicular to $\vec{E}$. The x-offset correction was made in the offline analysis, and both uncertainties were included in our systematic error estimate. The chamber ($\vec{E}$) was parallel to the magnet pole faces (perpendicular to $\vec{B}$) to within ±0.070°. Since the effective magnetic field is given by the product of B and the

cosine of this angle, the error could be neglected.

2.4) DATA ACQUISITION

The flow of the data acquisition electronics is shown in Figure 4. The Hamamatsu photodiode was biased with +40v producing a depletion region of ~300μm. The diode signal was amplified near the diode by a Laben 5240 hybrid preamplifier and amplified by an additional factor of 20 by an LRS333 NIM module. The diode signal provided the start for an LRS2228A 11 bit CAMAC TDC which was modified to provide a 5μs full scale. A coincidence was formed between the delayed diode signal and the chamber's anode signal, such that the arrival of the anode signal always determined the time of the coincidence output. This signal was used to stop the TDC and to gate an LRS2249A CAMAC ADC. The gate was tightly correlated in time to the arrival of the 8 pad signals. An IBM PC continuously searched for a LAM signal from the TDC via a Transiac 6002 CAMAC crate controller. If the LAM signal was detected, the PC inhibited further triggers through a CAMAC output register and searched for a LAM signal from the ADC. If this LAM was also found, the TDC and ADC were read out and histograms of the diode-anode time difference and the pad centroid were incremented. For each B and E field setting, data points were taken at the NEAR and FAR chamber positions and normally 1000 events were recorded at each data point. The time difference and pad centroid distributions were approximately gaussian with typical sigmas of 35ns and 2.2mm, so the statistical errors on the means of the distributions were typically 1.1ns and 0.070mm.

Triggers occurred at ~2hz at B=0 and increased to >100hz for B>10kG due to a helpful focussing of the electrons from the source. Because of the low rate very little data was taken at B=0. The IBM PC limited the maximum data acquisition rate to ~10hz.

The room temperature and absolute pressure were monitored throughout the data taking. We were primarily interested in relative values of these quantities between measurements and made no attempt to calibrate the mercury thermometer and Wallace-Tiernan model 61A-1A-0035 pressure gauge.

At least 5 complete volume exchanges with a new gas mixture were required before measurements were resumed. We were able to reproducibly go back and forth between pure AR/ET(50/50) and AR/ET(50/50) bubbled through alcohol at various temperatures. A gas entering the aluminum alcohol container passed through a diffusser with 1mm diameter holes which rested on the bottom of the container beneath 7.6cm of alcohol. Heat was removed from the system via a cold plate upon which the container sat, and all sides of the container were well insulated with styrofoam. The temperature of the alcohol was monitored to an accuracy of 0.1°C by a probe with remote readout manufactured by Solotron. The temperature was kept uniform throughout the alcohol volume by the mixing action of the bubbling gas.

2.5) SUMMARY OF EXPERIMENTAL ERRORS

The systematic errors due to alignment were explained in Section 2.3. One additional error which we consider an overall systematic error is a 2.5ns uncertainty in ΔTDC of Eq. 2 due to the TDC calibration.

Data was taken with our preferred gas on three separate occasions over a period of several days. Fortunately, the room temperature was constant to ±0.3°C and the absolute pressure to ±0.03psia, and the data sets were compared to measure the stability of the system. We found that Δx was reproducible to ±0.2mm and ΔTDC to ±1ns. For all data sets these uncertainties were added in quadrature to the statistical errors to produce "reproducibility errors", which are the first errors listed in the tables of

the next section. The overall systematic errors due to alignment and TDC calibration are listed separately.

The systematic errors in the quoted electric fields are explained in Section 2.2. The 1% absolute uncertainty in E was not included in the quoted errors for tan(η) and v, but was included in the systematic error for the quantity k which is defined in Section 4 and is directly proportional to the electric field. Errors due to electric field reproducibility are negligible.

The magnetic field was monitored with an NMR probe and was accurate and stable over the measurement region to 0.04% (eg, 0.006kG at 15kG). There was one exception to the direct NMR monitoring. For the AR/METHANE(80/20) measurements at 5kG, the magnet's current setting was calculated from the 10kG and 15kG values, and the uncertainty in B for this data is 1% (0.050kG).

3) RESULTS AND APPLICATIONS TO CDF OPERATION

3.1) CTC OPERATING POINT WITH THE PREFERRED GAS

For AR/ET(50/50) bubbled through ethyl alcohol at -7.2°C, v and tan(η) are presented as functions of E at B=10kG, 13.5kG, and 15kG in Table 1 and in Figures 6 and 7. For the purpose of reducing our results to a form amenable to calculation at intermediate values of the electric drift field E, we have fit v and tan(η) data to interpolation polynomials, and display the results in Table 2. The smooth curves plotted on Figures 6 and 7 are the results of the fits. The forms of our fit polynomials have no particular physical significance, and an attempt to extrapolate these

outside the range of our measurements leads quite rapidly to very wrong predictions. The desired CTC operating condition, $\tan(\eta)=1$, is however within the valid fit range, and solution of the fit polynomial for this condition gives $\tan(\eta)(E=1.35)=1.$, and $v(E=1.35)=51.2\mu m/ns$.

3.2) SENSITIVITY TO E, B, AR/ET RATIO, and ALCOHOL TEMPERATURE

We would like to limit the average error in measured position due to variations in any single operating parameter, such as alcohol temperature, to 25μm (σ per wire). For small changes in v and $\tan(\eta)$, the position error is approximately given by

Eq. 3 $\Delta pos \approx (\text{drift distance}) \cdot [\Delta v/v - \tan(\theta)\Delta\tan(\eta)]$,

where Δv and $\Delta\tan(\eta)$ are the changes in velocity and $\tan(\eta)$ and θ is the angle of the track with respect to the radial direction. Note that the position error is sensitive only to velocity changes for approximately radial, high p_T tracks. For each of the operating parameters (β = E, B, argon fraction, and alcohol temperature), Table 3 lists the measured gradients $\Delta v/\Delta\beta$ and $\Delta\tan(\eta)/\Delta\beta$ and the gradients $\Delta pos/\Delta\beta$ which were calculated from Eq. 3 for our average drift distance of 1.75cm and $|\theta|$ = 0°, 22.5°, and 45°. The sign of θ was always chosen to give the maximum position error.

The gradients $\Delta v/\Delta E$ and $\Delta\tan(\eta)/\Delta E$ were estimated from the fit polynomials and are given in Table 3a. In order to limit position errors to 25μm, the operating tolerance in E is a managable 0.9% for radial tracks. The tolerance for 45° tracks, 0.1% of E, will be more difficult to achieve but is also much less critical to the chamber's performance.

Our measurements show that the dependence of the two quantities v and tan(η) on the magnetic field B at the two electric field data points nearest the suggested operating point E=1.35kV/cm is linear. The slopes listed in Table 3b are therefore resulting from a linear fit to the three magnetic field data points at each of the two electric field settings. In order to limit position errors to 25μm allowing for the worst case 2σ variation in Δpos/Δβ, the operating tolerance in B is 0.45kG for radial tracks and 0.04kG for tracks with θ=22.5°. Since the CTC wires will extend to regions in magnetic field that are 0.30kG below the nominal 15kG at center of the detector, a correction for tracks with significant θ should be considered.

In order to study the effect of variations in gas ratio, measurements of v and tan(η) were made at 15kG with AR/ET gas mixtures of 40/60, 48/52, and 52/48 bubbled through alcohol at -7.2°C. These measurements are presented in Table 4. Comparison of the results of the 48/52 and 52/48 data with the 50/50 results presented in Table 1, demonstrate a rather slow dependence on the precise gas mixture of our measured quantities. The slopes listed in Table 3c are from linear fits to the data points at E=1.476kV/cm. Allowing for the worst case 2σ variation in Δpos/Δβ, the gas mixing system should keep the argon fraction within 0.0055 of nominal in order to assure position errors of less than 25μm for radial tracks.

Results from data taken using AR/ET(50/50) at B=15kG with alcohol temperatures (alcohol percentages[3]) of -3.1°C (1.29%), -7.2°C (0.98%), and -11.2°C (0.74%) are presented in Tables 1 and 5. Figures 8 and 9 show v and tan(η) as functions of E for this data and for AR/ET(50/50) without alcohol. There are substantial changes in the drift parameters due to small changes

in alcohol concentration, particularly in tan(η) at small E. The data at the two electric field values closest to the operating value were fit to straight lines and the resulting values of slope and the calculated position gradients are given in Table 3d. The tolerance for 25μm error is approximately -0.5°C for radial tracks, -0.2°C for 22.5° tracks, and -0.1°C for 45° tracks. For the actual CTC bubbling system, we plan to immerse the alcohol container into an antifreeze bath inside the Neslab RTE-9DD refrigerator which maintains the bath temperature to ±0.01°C.

3.3) AR/ET(50/50) WITHOUT ALCOHOL, HRS GAS, AR/METHANE(80/20)

Tables 6, 7, and 8 give the results of measurements with pure AR/ET(50/50), "HRS gas" [AR/CO_2/METHANE(88.96/10.08/0.96)], and AR/METHANE(80/20). The first two gases were tested as possible alternatives to the preferred CTC gas. As seen in the tables, at 15kG both gases have well saturated velocities in E at tan(η)=1.0 with operating electric fields of 1.60kV/cm for AR/ET(50/50) and 1.31kV/cm for HRS gas. As noted earlier we would like to avoid using pure AR/ET(50/50) due to the polymerization problem.

The AR/METHANE(80/20) mixture was tested with limited success for CDF's VTPC chamber which operates inside the CTC in a 15kG magnetic field. The electric field is parallel to the magnetic field in the VTPC'c drift region, but perpendicular components arise in the readout portion of the chamber. The test chamber was unable to reach a high enough electric field in this gas to allow data to be taken at 15kG. The data at 5kG and 10kG show that the Lorentz angle is much larger at the same electric field than for the other tested gases and that there is no saturation of velocity with electric field.

4) COMPARISONS TO THE THEORY OF ELECTRON DRIFT

The drift velocity and angle of electrons in a gas in the presense of an electric field and a perpendicular magnetic field are given by[4]

Eqs. 4
$$v_L=(1+\omega^2\bar{\tau}^2)^{-1}\,[(2/3)(eE/m)\langle L/\nu\rangle+(1/3)(eE/m)\langle dL/d\nu\rangle],$$
$$=(1+\omega^2\bar{\tau}^2)^{-1}\,v_o, \text{ and}$$
$$v_T=(1+\omega^2\bar{\tau}^2)^{-1}\,[(1/3)(eE/m)\omega\langle(L/\nu)^2\rangle+(2/3)(eE/m)\omega\langle(L/\nu)(dL/d\nu)\rangle],$$

where v_L [v_T] is the component of the drift velocity which is parallel (transverse) to the electric field, v_o is the drift velocity at B=0, $\omega=(eB/m)$, ν is the electron velocity, τ is the effective time between collisions, L is the mean free path, and the angle brackets refer to the average over electron energies; for example,

$$\langle L/\nu\rangle = \int[L(\varepsilon)/\nu]F(\varepsilon)d\varepsilon, \text{ where } \varepsilon=(1/2)m\nu^2.$$

Given $L(\varepsilon)$, $F(\varepsilon)$ can be found from the Boltzman transport equation, thus allowing v_L and v_T to be calculated from Eqs. 4. This has been done successfully for pure argon for which the ion cross section as a function of energy is well measured,[4] but for most gases the cross sections are unknown.

For electric field values small enough so that the average electron energy is not significantly increased from the thermal value, the electron mobility ($\mu=v_o/E$) is constant.[5] This is realized in Eqs. 4 when τ is constant:

Eqs. 5
$$(dL/d\nu)=L/\nu=\bar{\tau}, \quad v_o=(eE/m)\bar{\tau},$$
$$v_L=(1+\omega^2\bar{\tau}^2)^{-1}\,(eE/m)\bar{\tau}, \quad v_T=v_L\omega\bar{\tau},$$
$$v=v_o(1+\omega^2\bar{\tau}^2)^{-1/2}, \text{ and}$$
$$\tan(\eta)=\omega\bar{\tau}=(Bv_o/E)=(Bv/E)[1+\tan^2(\eta)]^{1/2}.$$

In the data tables we list the quantity

$$k=\{Bv/E[\tan(\eta)]\}[1+\tan^2(\eta)]^{1/2},$$

which should equal 1 for all B if this special case is valid. For all the gases tested, k monotonically increases toward 1 as E decreases. At the lowest measured field, E=0.49kV/cm, k≈0.95 for the preferred mixture (Table 1) and k≈0.98 for the HRS mixture (Table 7). Eqs. 5 also predict that tan(η) is independent of electric field. For the HRS gas at 15kG, as E decreases from 1.72kV/cm, tan(η) increases until E≈0.7kV/cm and then begins to decrease. This indicates that the special case is not realized in detail at E=0.7kV/cm for the HRS mixture.

In Figures 10 and 11 our AR/ET(50/50) data at B=0, 10kG, and 15kG are compared with data from Daum et al.[1] and with the model predictions of Ramanantsizehena.[5,6] Figures 10a, 10b, and 10c show the drift velocity as a function of electric field at the three magnetic field values. The two data sets are consistent within errors at B=0 and B=15kG, but disagree by many standard deviations below E=1400V/cm at B=10kG. With the exception of the Daum et al. points in this region, the velocity data are quite well described by the model. Figure 11 is a plot of the Lorentz angle, η, as a function of E for B=5kG, 10kG, and 15kG. The two data sets are in fair agreement, but the model predictions fall considerably below the data at 10kG and 15kG.

5) CONCLUSIONS AND ACKNOWLEDGEMENTS

We have described an experiment which measured electron drift velocities and Lorentz angles in several gases up to B=15kG, primarily to determine operating parameters for the Central Tracking Chamber in CDF. The data were compared to the theory of electron drift in gases at small electric field. The preferred gas and HRS gas appear to closely approach this regime as E falls below 0.5kV/cm. The AR/ET(50/50) data at B=0, 10kG, and 15kG show fairly good agreement with earlier experimental results and with a model based on the general theory of electron drift in gases.

We would like to acknowledge useful discussions with Peter Berge, the fine technical support of Michael Hrycyk and Walter Coleman, the precise machining of Bernie Bowker, Jack Layman, and Jerry Knopf, and the dedicated efforts of the Fermilab personnel who installed the magnet. Fermilab is operated by the Universities Research Association under contract with the U.S. Department of Energy.

References

1. H. Daum et al., Nucl. Instr. and Meth. 152 (1978) 541.
2. M. Atac, IEEE Trans. on Nucl. Sci. , NS-31 (1984) 99.
3. R. Weast, editor, CRC Handbook of Chemistry and Physics, CRC Press, Cleveland, Ohio (1972).
4. V. Paladino and B. Sadoulet, LBL Internal Report, LBL-3013 (1974).
5. A. Peisert and F. Sauli, CERN Report, CERN 84-08 (1984).
6. P. Ramanantsizehena, Thesis, University of Strasbourg, CRN-HE-99-13 (1979).

Table 1 -- Preferred Gas - v and tan(η) versus E and B

The dependence of v and tan(η) on E and B for our preferred gas, AR/ET(50/50) bubbled through alcohol at -7.2°C. The average room temperature and average absolute air pressure for each data set are given inside the square brackets. The errors in v, tan(η), k, E, and B are described in Section 2.5.

E (kV/cm)	tan(η)	v (μm/ns)	k
	10kG [24.5°C, 14.35psia]		
1.722	0.4582±0.0042±0.0018	51.792±0.111±0.123	.722±.004±.008
1.476	0.5381±0.0042±0.0019	51.972±0.120±0.121	.743±.003±.008
1.230	0.6448±0.0042±0.0020	51.590±0.123±0.115	.744±.002±.008
0.984	0.7960±0.0043±0.0021	49.974±0.123±0.102	.815±.001±.008
0.738	0.9655±0.0043±0.0024	45.018±0.112±0.078	.878±.001±.009
0.492	1.1631±0.0043±0.0027	34.877±0.086±0.046	.935±.001±.009
	13.5kG [24.5°C, 14.36psia]		
1.722	0.6635±0.0043±0.0020	51.937±0.128±0.115	.736±.002±.008
1.476	0.7925±0.0043±0.0021	51.957±0.130±0.110	.765±.001±.008
1.230	0.9576±0.0043±0.0024	50.733±0.127±0.098	.805±.001±.008
0.984	1.1698±0.0044±0.0027	47.618±0.118±0.079	.859±.001±.009
0.738	1.4036±0.0043±0.0033	40.918±0.093±0.055	.919±.001±.009
0.492	1.5782±0.0044±0.0037	29.314±0.067±0.029	.952±.002±.010
	15kG [24.5°C, 14.38psia]		
1.722	0.7690±0.0043±0.0021	52.150±0.131±0.112	.746±.001±.008
1.476	0.9104±0.0043±0.0023	51.712±0.131±0.103	.781±.001±.008
1.230	1.1051±0.0043±0.0026	50.288±0.124±0.090	.827±.001±.008
0.984	1.3324±0.0044±0.0031	46.257±0.109±0.070	.882±.001±.009
0.738	1.5823±0.0044±0.0038	38.827±0.086±0.046	.934±.001±.009
0.492	1.7142±0.0047±0.0042	26.918±0.074±0.024	.950±.001±.010

Table 2 -- Fits of v and tan(η) as functions of E for the preferred gas
Fits of a) v and b) $[\tan(\eta)]^{-1}$ to polynomials in E for the preferred gas at several magnetic fields. The units of v and E in the fits are μm/ns and kV/cm, respectively. The fits are plotted with the data in Figures 6 and 7.

B (kG)	α_1	α_2	α_3	α_4	χ^2 (2df)
a) $v = \sum \alpha_i E^{i-1}$, i=1 to 4					
10	-6.87 ± 1.15	120.92 ± 3.92	-82.46 ± 3.96	18.60 ± 1.22	2.34
13.5	-13.64 ± 1.03	119.53 ± 3.50	-72.77 ± 3.57	14.79 ± 1.11	1.16
15	-14.86 ± 0.99	113.56 ± 3.36	-64.22 ± 3.42	12.11 ± 1.07	0.90
b) $[\tan(\eta)]^{-1} = \sum \alpha_i E^{i-1}$, i=1 to 4					
10	0.745 ± 0.065	-0.127 ± 0.231	0.806 ± 0.249	-0.143 ± 0.082	2.15
13.5	0.720 ± 0.034	-0.566 ± 0.118	0.875 ± 0.126	-0.164 ± 0.041	0.33
15	0.744 ± 0.028	-0.752 ± 0.096	0.960 ± 0.101	-0.195 ± 0.033	2.05

Table 3 -- Effect of Parameter Variations on v, tan(η), and Position
The table gives the gradients of v and tan(η) with respect to a) E, b) B, c) argon fraction, and d) alcohol temperature for our preferred gas. Also listed are position resolution gradients (Δpos/Δβ) calculated from Eq. 3 for the CTC's average drift distance of 1.75cm and $|\theta|$=0°, 22.5°, and 45°. The sign of θ was always chosen to maximize $|\Delta pos/\Delta\beta|$.

E (kV/cm)	Δv/Δβ μm/ns/β-unit	Δtan(η)/Δβ (β-unit)$^{-1}$	TRACK ∢(°)	Δpos/Δβ(max) (μm/β-unit)
		a) β = E (kV/cm)		
1.350	6.30	-.770	0(radial)	2153.
			22.5	7734.
			45.0	15628.
		b) β = B (kG)		
1.476	-0.042±0.034	0.0742±0.0012	0	14.5±11.7
			22.5	553.±14.5
			45.0	1307.±24.0
1.230	-0.258±0.034	0.0916±0.0012	0	88.2±11.6
			22.5	752.±14.5
			45.0	1691.±24.0
		c) β = ARGON FRACTION		
1.476	-3.95±4.70	-0.0532±0.1538	0	1350.±1606.
			22.5	1736.±1955.
			45.0	2281.±3134.
		d) β = ALCOHOL TEMPERATURE (°C)		
1.476	-0.112±0.023	-0.0124±0.0008	0	38.3±7.9
			22.5	128.±9.8
			45.0	255.±16.0
1.230	-0.162±0.022	-0.0179±0.0008	0	55.4±7.5
			22.5	185.±9.8
			45.0	369.±15.9

Table 4 -- Sensitivity to AR/ET Ratio

The sensitivity of v and tan(η) to the AR/ET ratio at 15kG. The gas mixtures were bubbled through alcohol at -7.2°C. Data for AR/ET(50/50) are found in Table 1. The average room temperature and average absolute air pressure for each data set are given inside the square brackets. The errors in v, tan(η), k, E, and B are described in Section 2.5.

E (kV/cm)	tan(η)	v (μm/ns)	k
	AR/ET(48/52) [24.0°C, 14.40psia]		
1.722	0.7639±0.0043±0.0021	52.091±0.131±0.112	.747±.002±.008
1.476	0.9162±0.0044±0.0023	51.925±0.133±0.104	.781±.001±.008
	AR/ET(52/48) [24.0°C, 14.41psia]		
1.722	0.7593±0.0043±0.0021	51.802±0.131±0.111	.746±.002±.008
1.476	0.9140±0.0044±0.0023	51.767±0.133±0.104	.780±.001±.008
	AR/ET(40/60) [24.0°C, 14.37psia]		
1.722	0.7683±0.0042±0.0021	53.056±0.133±0.115	.759±.002±.008
1.476	0.9093±0.0042±0.0023	52.284±0.129±0.106	.790±.001±.008
1.230	1.0844±0.0043±0.0026	50.216±0.122±0.091	.833±.001±.008
0.984	1.2939±0.0043±0.0030	45.915±0.109±0.070	.885±.001±.009
0.738	1.5115±0.0043±0.0036	38.218±0.085±0.046	.931±.001±.009

Table 5 -- Sensitivity to Alcohol Temperature

The sensitivity of v and tan(η) to alcohol temperature at 15kG for AR/ET(50/50) bubbled through alcohol. Data for the preferred alcohol temperature of -7.2°C are listed in Table 1. The average room temperature and average absolute air pressure for each data set are given inside the square brackets. The errors in v, tan(η), k, E, and B are described in Section 2.5.

E (kV/cm)	tan(η)	v (μm/ns)	k
	-3.1°C [24.5°C, 14.39psia]		
1.722	0.7370±0.0043±0.0021	51.825±0.127±0.112	.761±.002±.008
1.476	0.8638±0.0043±0.0022	51.296±0.129±0.104	.797±.001±.008
1.230	1.0336±0.0043±0.0025	49.457±0.120±0.090	.839±.001±.009
0.984	1.2378±0.0043±0.0029	45.505±0.105±0.071	.892±.001±.009
0.738	1.4306±0.0043±0.0033	37.939±0.084±0.047	.941±.001±.009
	-11.2°C [24.5°C, 14.38psia]		
1.722	0.7960±0.0043±0.0021	52.140±0.134±0.110	.729±.001±.007
1.476	0.9644±0.0044±0.0024	52.202±0.135±0.103	.764±.001±.008
1.230	1.1784±0.0044±0.0027	50.761±0.127±0.089	.812±.001±.008
0.984	1.4488±0.0044±0.0034	47.078±0.110±0.069	.872±.001±.009
0.738	1.7560±0.0045±0.0043	39.659±0.088±0.045	.928±.002±.009

Table 6 -- AR/ET(50/50) - v and tan(η) versus E and B

The dependence of v and tan(η) on E and B for pure AR/ET(50/50). The average room temperature and average absolute air pressure for each data set are given inside the square brackets. The errors in v, tan(η), k, E, and B are described in Section 2.5.

E (kV/cm)	tan(η)	v (μm/ns)	k
		0kG [26.0°C, 14.36psia]	
1.476		51.302±0.100±0.130	
0.738		52.263±0.100±0.134	
0.246		41.597±0.077±0.085	
		10kG [26.0°C, 14.36psia]	
1.722	0.5041±0.0042±0.0019	51.316±0.116±0.119	.662±.003±.007
1.476	0.6193±0.0042±0.0019	52.217±0.126±0.119	.672±.002±.007
1.230	0.7911±0.0043±0.0021	52.915±0.135±0.114	.693±.001±.007
0.984	1.0228±0.0044±0.0025	52.690±0.140±0.102	.749±.001±.008
0.738	1.3546±0.0045±0.0031	49.086±0.129±0.077	.827±.001±.008
		15kG [26.0°C, 14.33psia]	
1.722	0.8955±0.0043±0.0023	52.785±0.140±0.108	.689±.001±.007
1.476	1.1086±0.0044±0.0026	52.929±0.137±0.099	.724±.001±.007
1.230	1.4213±0.0045±0.0033	52.510±0.133±0.085	.783±.001±.008
1.126	1.5760±0.0045±0.0037	51.337±0.123±0.077	.810±.001±.008

Table 7 -- HRS Gas - v and tan(η) versus E and B

The dependence of v and tan(η) on E and B for HRS gas. The average room temperature and average absolute air pressure for each data set are given inside the square brackets. The errors in v, tan(η), k, E, and B are described in Section 2.5.

E (kV/cm)	tan(η)	v (μm/ns)	k
		13.5kG [24.0°C, 14.43psia]	
1.476	0.7808±0.0043±0.0021	50.915±0.139±0.106	.757±.002±.008
1.230	0.9263±0.0043±0.0023	51.404±0.131±0.102	.830±.001±.008
0.984	1.0747±0.0043±0.0026	48.744±0.124±0.086	.913±.001±.009
0.738	1.1463±0.0043±0.0027	39.880±0.096±0.058	.968±.001±.010
		15kG [24.0°C, 14.40psia]	
1.476	0.8939±0.0044±0.0023	51.072±0.138±0.102	.779±.001±.008
1.230	1.0550±0.0044±0.0025	50.906±0.132±0.094	.855±.001±.009
0.984	1.2153±0.0043±0.0028	47.257±0.116±0.077	.933±.001±.009
0.738	1.2607±0.0043±0.0029	37.552±0.087±0.050	.974±.001±.010
0.492	1.1711±0.0042±0.0027	24.430±0.056±0.025	.979±.001±.010

Table 8 -- AR/METHANE(80/20) - v and tan(η) versus E and B

The dependence of v and tan(η) on E and B for AR/METHANE(80/20). The average room temperature and average absolute air pressure for each data set are given inside the square brackets. The errors in v, tan(η), k, E, and B are described in Section 2.5.

E (kV/cm)	tan(η)	v (μm/ns)	k
	5kG [24.5°C, 14.30psia]		
1.722	0.2466±0.0044±0.0017	37.756±0.080±0.069	.458±.007±.005
1.476	0.3013±0.0042±0.0018	39.541±0.074±0.075	.464±.005±.005
1.230	0.3918±0.0045±0.0018	42.028±0.104±0.083	.468±.004±.005
0.984	0.5650±0.0045±0.0019	46.021±0.125±0.095	.475±.002±.005
0.738	0.8909±0.0049±0.0023	53.709±0.168±0.112	.547±.001±.006
0.492	1.5879±0.0058±0.0038	63.823±0.221±0.114	.767±.002±.008
	10kG [24.0°C, 14.30psia]		
1.722	0.6326±0.0046±0.0020	39.884±0.106±0.071	.433±.002±.004
1.476	0.8452±0.0047±0.0022	43.535±0.124±0.077	.457±.001±.005
1.230	1.1812±0.0050±0.0028	48.901±0.144±0.083	.521±.001±.005

Figure Captions

Fig. 1 The Central Tracking Chamber as viewed from the beam (or axial) direction. The wires are divided into 9 super layers along the radial direction. The layers alternate between wires in the axial direction and wires at a ±3° stereo angle.

Fig. 2. A CTC super cell in an axial layer. The cell is tilted by 45° with respect to the radial direction to allow for electron drift in the ϕ direction at 15kG.

Fig. 3 An elevation view of the apparatus used to measure drift velocities and Lorentz angles at high magnetic field. Not shown is the precision slide and stepping motor which drove the u-channel and thereby the drift chamber in the x-direction. In order to move the chamber between its NEAR and FAR y-positions, the aluminum plate was rolled atop the u-channel on teflon balls.

Fig. 4 An illustration of the measurement procedure and data acquisition.

Fig. 5 a) An elevation view of the drift chamber used for the measurements of v and tan(η), including a calculation of the of the equipotential lines for HV=-9.5kV. b) The calculated electric field in the drift region as a function of the y-coordinate for HV=-9.5kV.

Fig. 6 The dependence of v on E for the preferred gas mixture. The curves are fits to the form $v=\sum\alpha_i E^{i-1}$ (i=1 to 4), and the fitted parameters are given in Table 2.

Fig. 7 The dependence of tan(η) on E for the preferred gas mixture. The curves are fits to the form $[\tan(\eta)]^{-1} = \sum\alpha_i E^{i-1}$ (i=1 to 4), and the fitted parameters are given in Table 2.

Fig. 8 The dependence of v on E at B=15kG for AR/ET(50/50) with several alcohol concentrations. The curves were drawn to guide the eye.

Fig. 9 The dependence of tan(η) on E at B=15kG for Ar/ET(50/50) with several alcohol concentrations. The curves were drawn to guide the eye.

Fig. 10 The dependence of v on E at a)B=0, b)B=10kG, and c)B=15kG for AR/ET(50/50). The curves are the predictions of Reference 6.

Fig. 11 The dependence of tan(η) on E at B=5kG, 10kG and 15kG for AR/ET(50/50). The curves are the predictions of Reference 6.

FIGURE 1

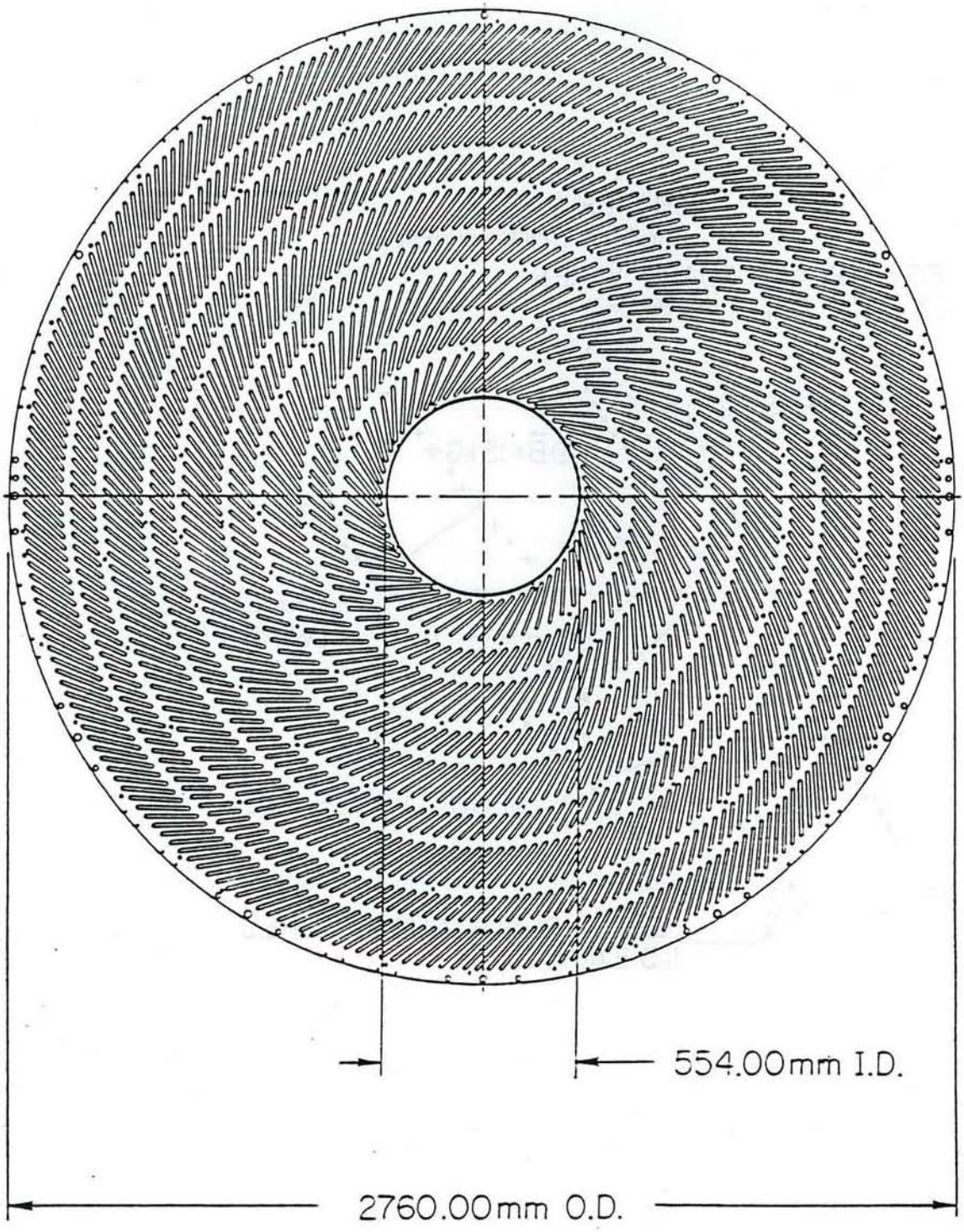

FIGURE 2

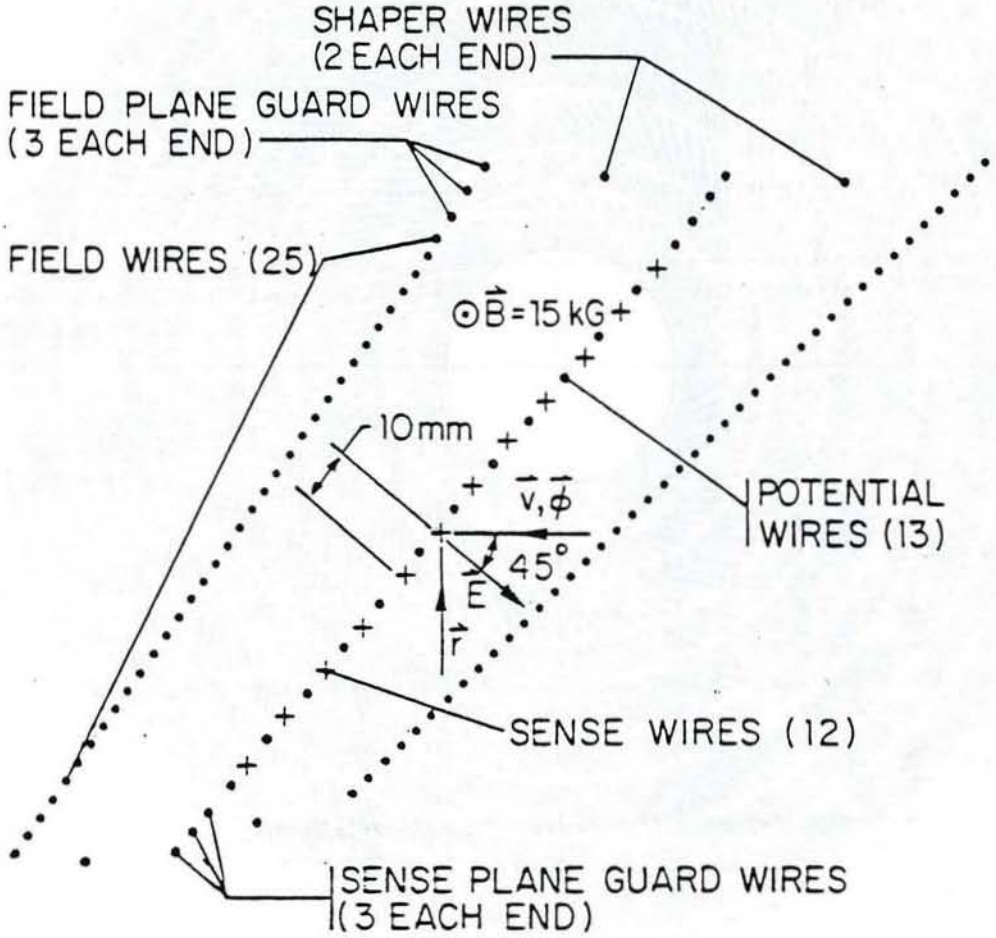
SHAPER WIRES
(2 EACH END)
FIELD PLANE GUARD WIRES
(3 EACH END)
FIELD WIRES (25)
⊙B=15 kG
10mm
v, ϕ
45°
E
r
POTENTIAL
WIRES (13)
SENSE WIRES (12)
SENSE PLANE GUARD WIRES
(3 EACH END)

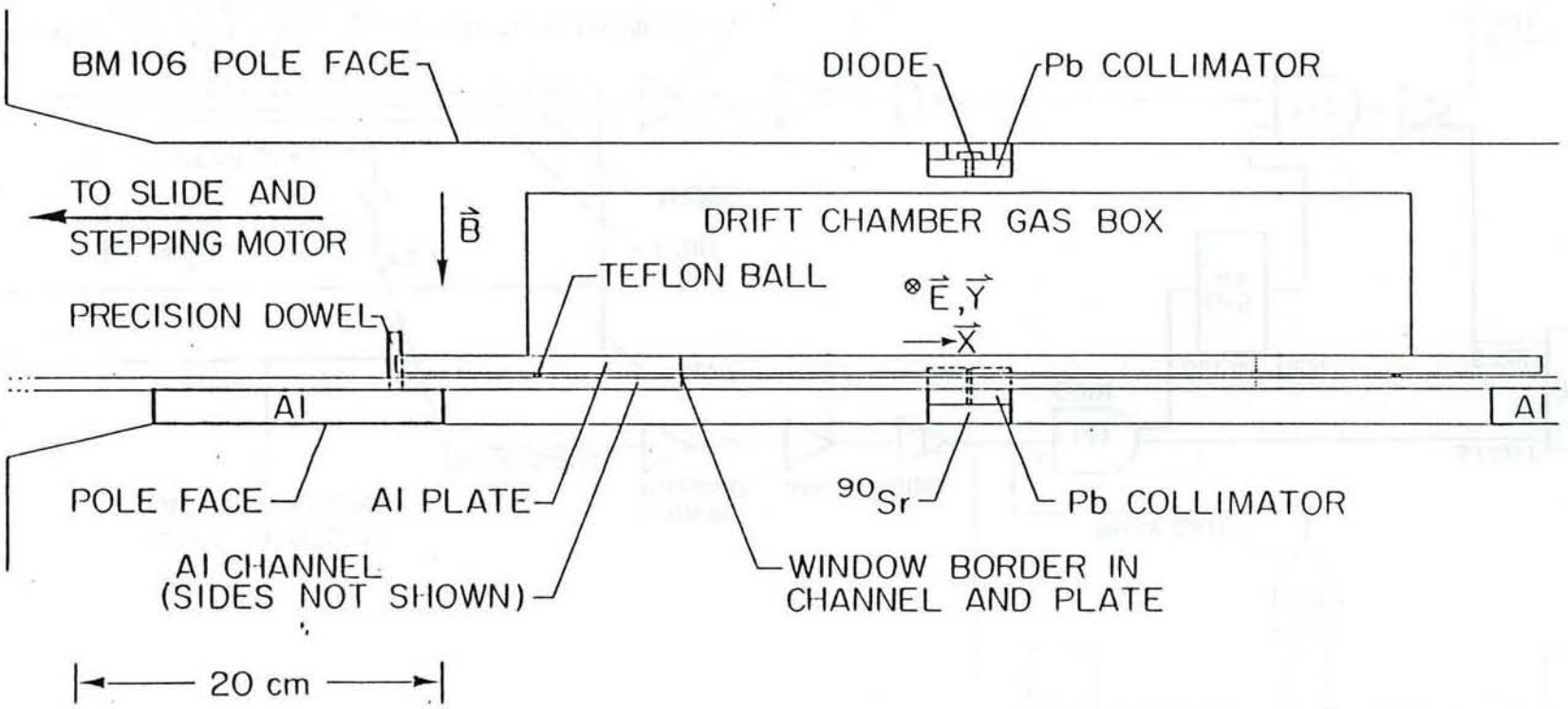
BM 106 POLE FACE
DIODE
Pb COLLIMATOR
TO SLIDE AND
STEPPING MOTOR
$\vec{B}$
DRIFT CHAMBER GAS BOX
TEFLON BALL
$\otimes \vec{E}, \vec{Y}$
$\rightarrow \vec{X}$
PRECISION DOWEL
Al
Al
POLE FACE
Al PLATE
^{90}Sr
Pb COLLIMATOR
Al CHANNEL
(SIDES NOT SHOWN)
WINDOW BORDER IN
CHANNEL AND PLATE
20 cm

FIGURE 5

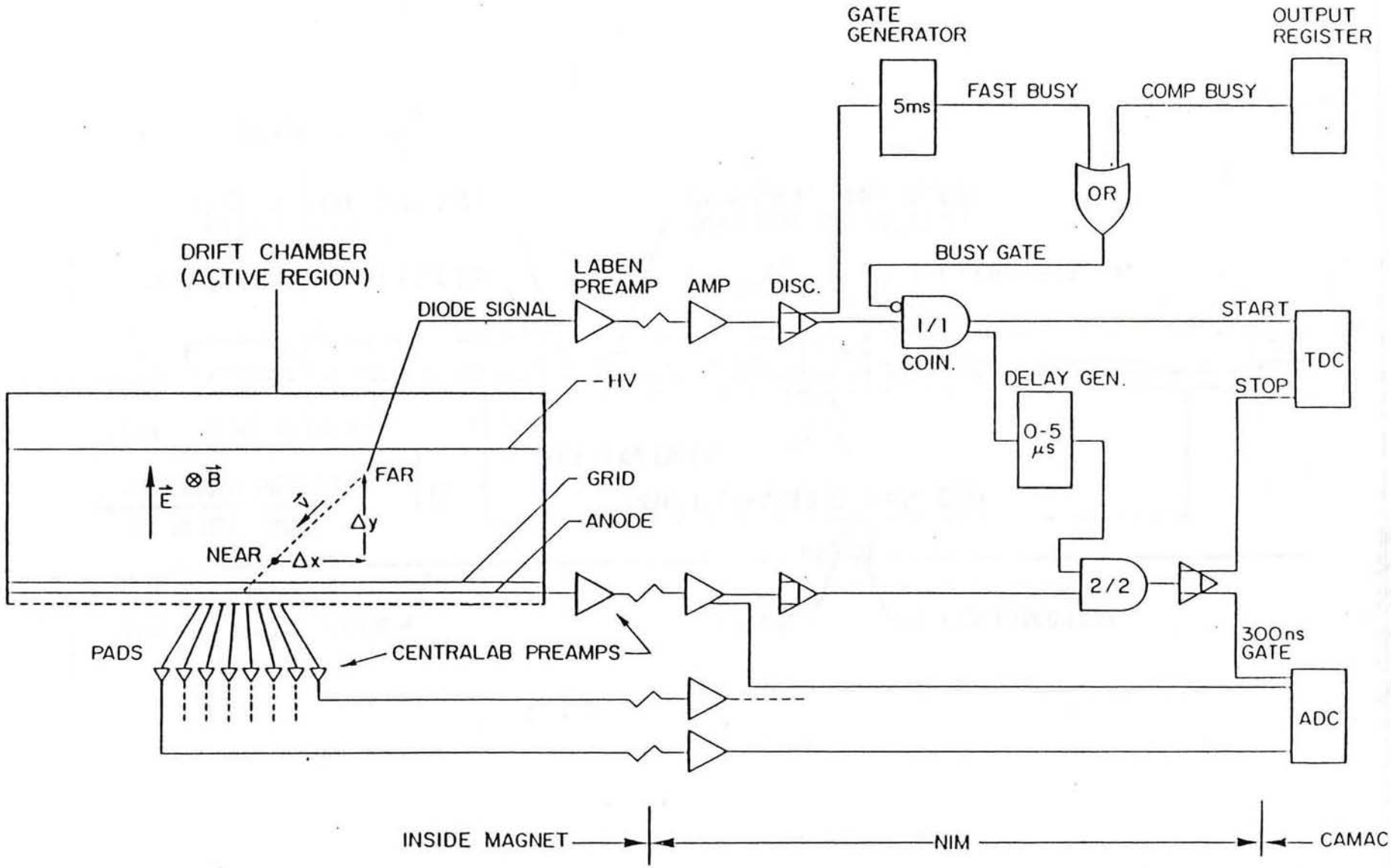
GATE GENERATOR
OUTPUT REGISTER
5ms
FAST BUSY
COMP BUSY
OR
BUSY GATE
DRIFT CHAMBER (ACTIVE REGION)
LABEN PREAMP
AMP
DISC.
DIODE SIGNAL
1/1
COIN.
START
TDC
DELAY GEN.
STOP
0-5 μs
HV
GRID
ANODE
FAR
NEAR
Δx
Δy
2/2
300ns GATE
PADS
CENTRALAB PREAMPS
ADC
INSIDE MAGNET
NIM
CAMAC

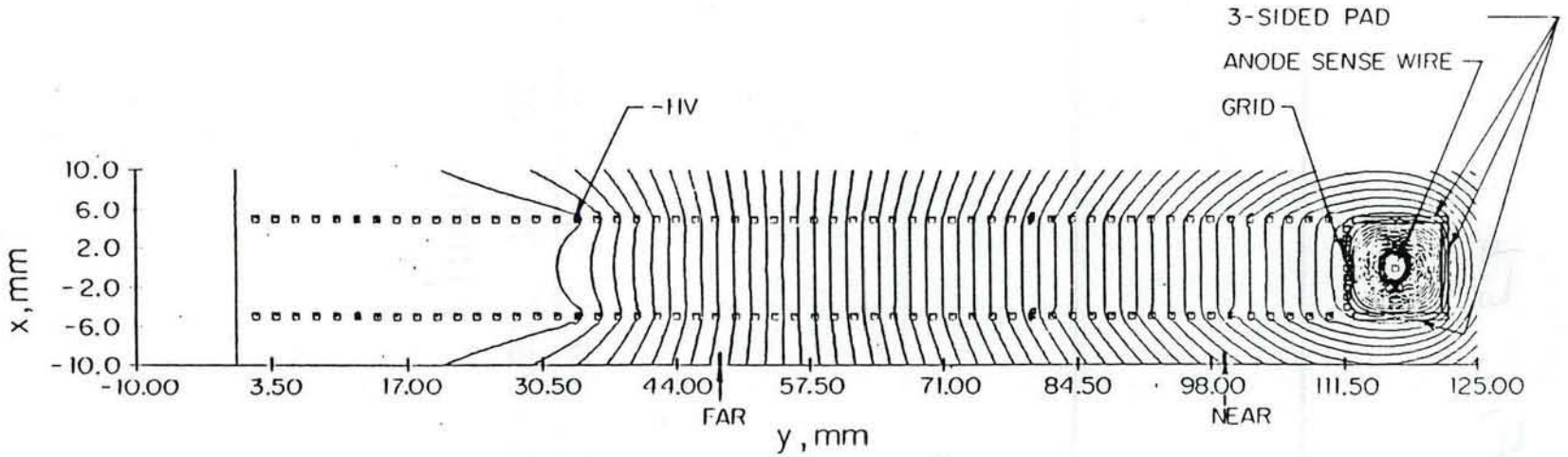
3-SIDED PAD
ANODE SENSE WIRE
GRID
-11V
10.0
6.0
2.0
-2.0
-6.0
-10.0
x, mm
-10.00
3.50
17.00
30.50
44.00
57.50
71.00
84.50
98.00
111.50
125.00
FAR
NEAR
y, mm

FIGURE 5a)

Fig. 5b

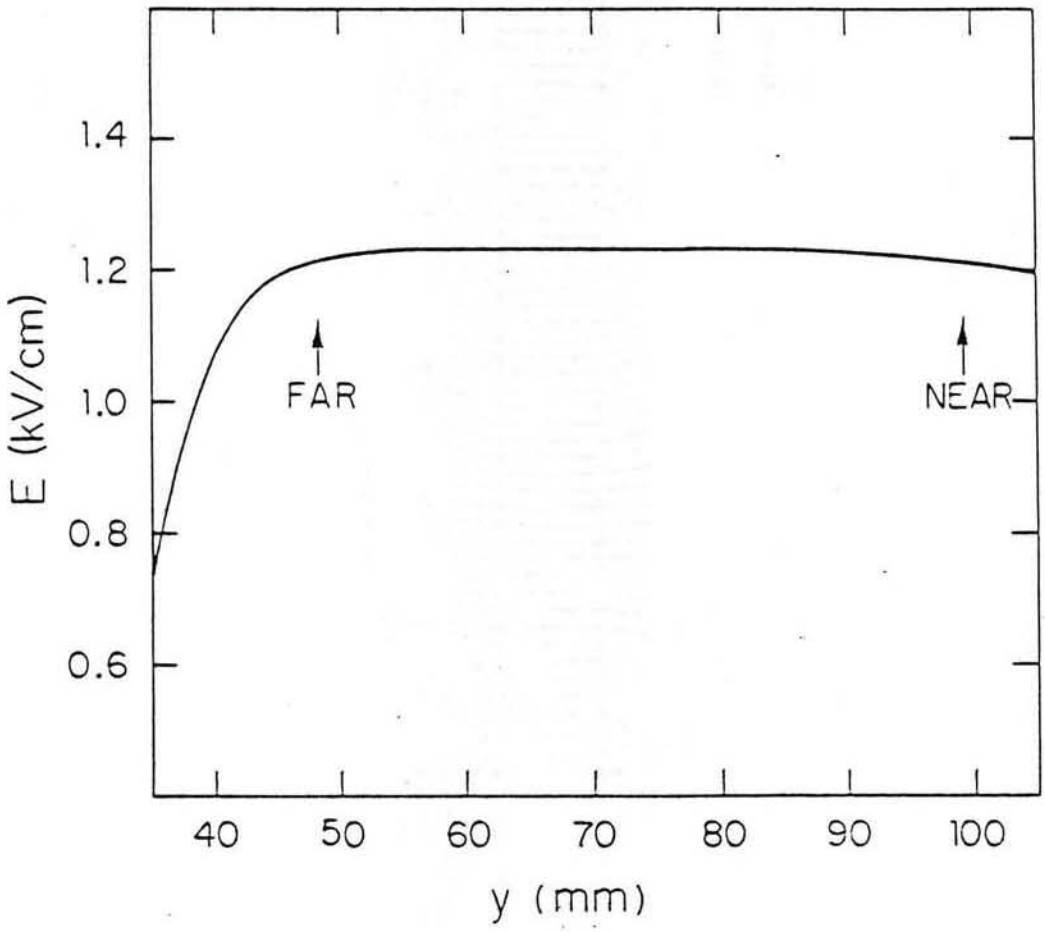

FIGURE 6

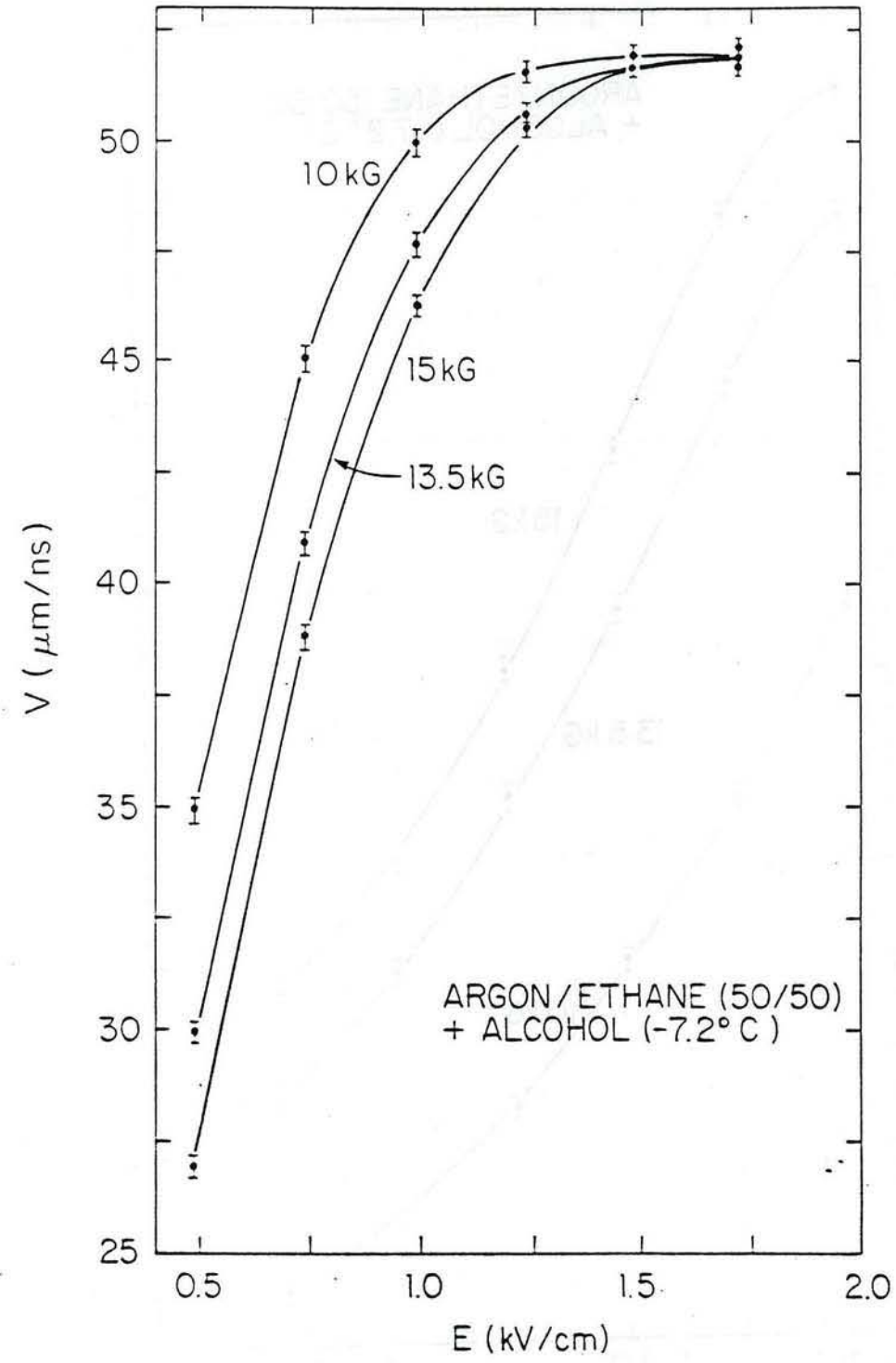
50
45
40
35
30
25
V (μm/ns)
10 kG
15 kG
13.5 kG
ARGON / ETHANE (50/50)
+ ALCOHOL (-7.2° C)
0.5
1.0
1.5
2.0
E (kV/cm)

FIGURE 7

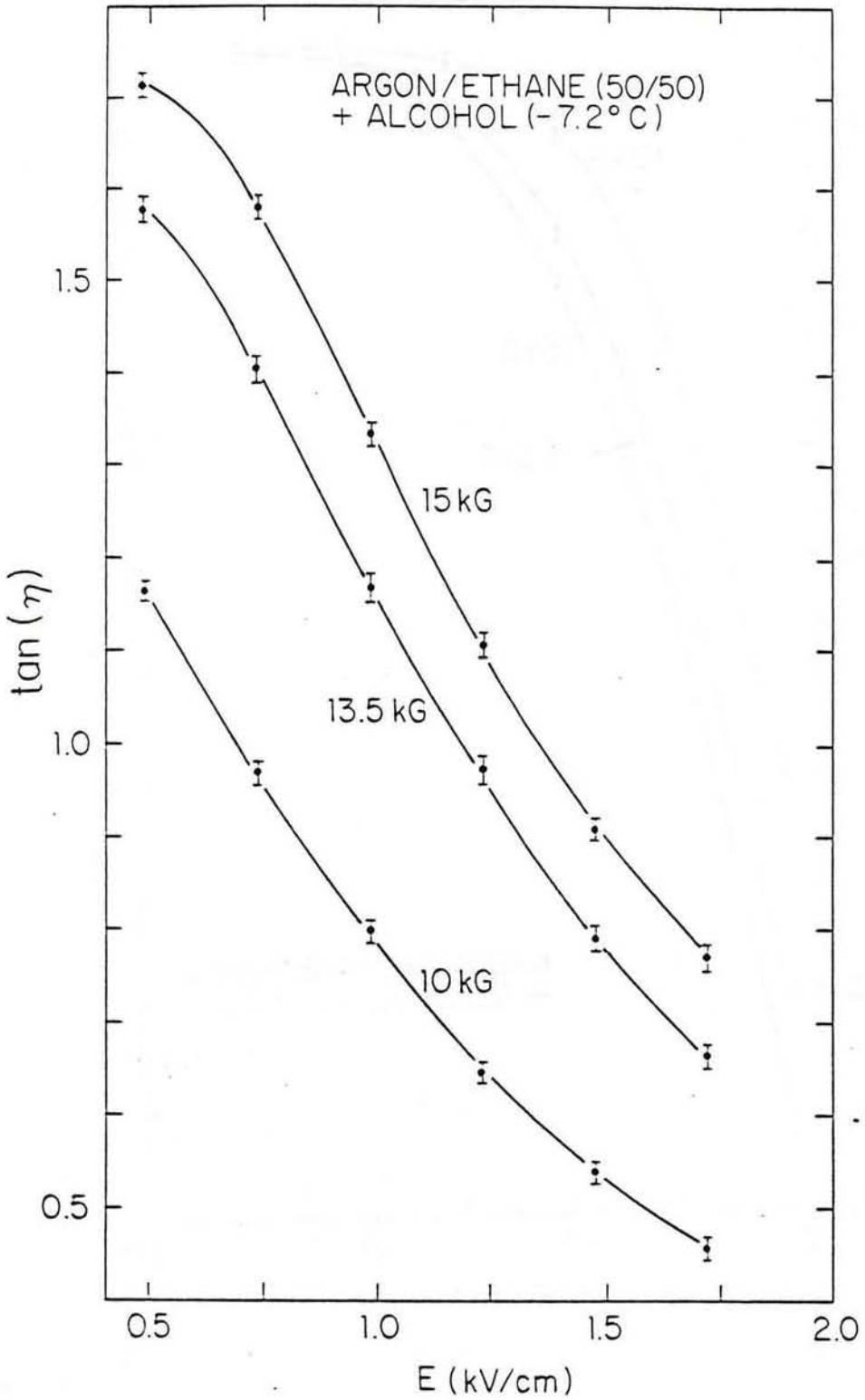
ARGON/ETHANE (50/50)
+ ALCOHOL (-7.2° C)
15 kG
13.5 kG
10 kG
tan (η)
1.5
1.0
0.5
0.5
1.0
1.5
2.0
E (kV/cm)

FIGURE 8

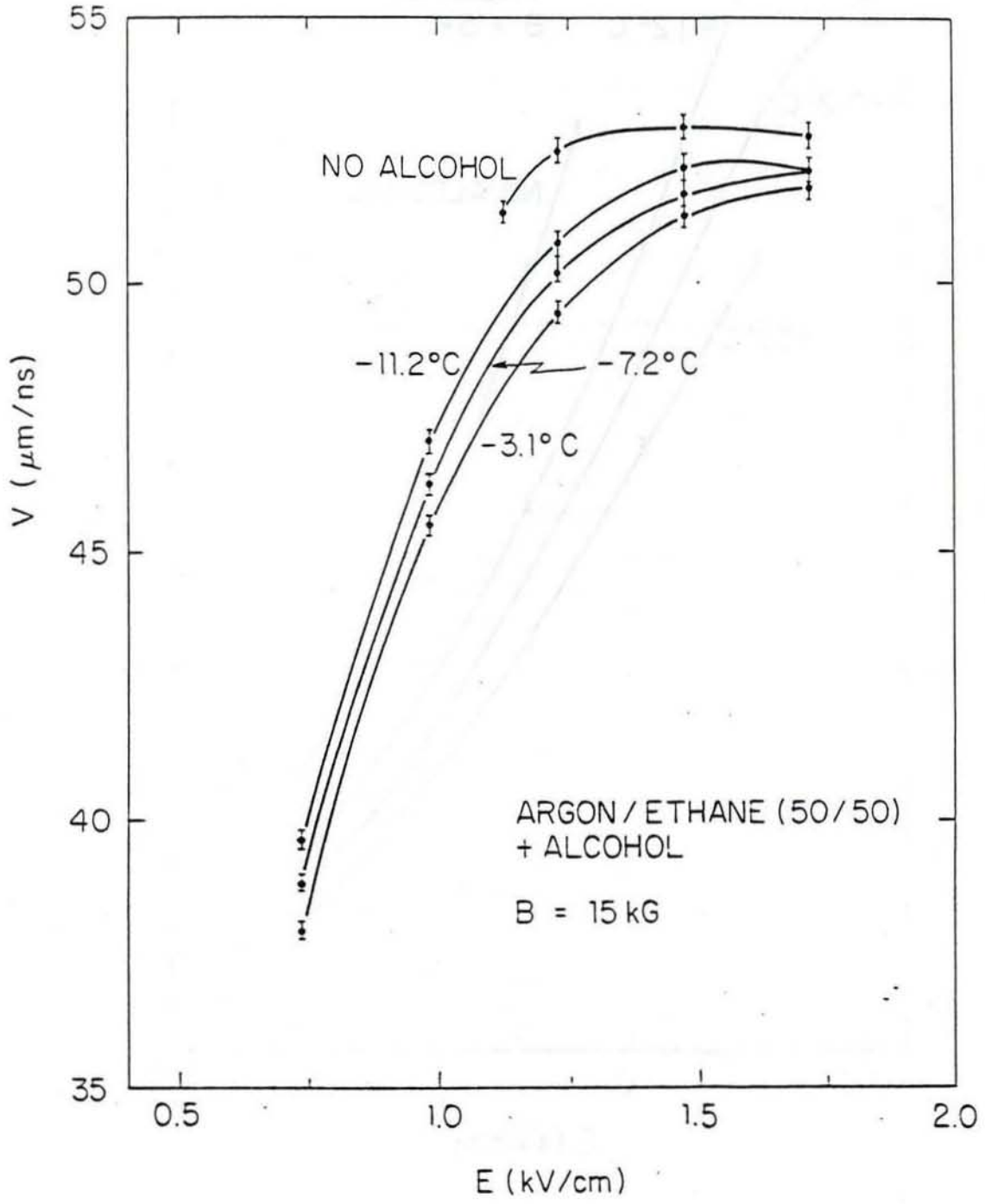
55
50
45
40
35
V (μm/ns)
NO ALCOHOL
-11.2°C
-7.2°C
-3.1° C
ARGON / ETHANE (50/50)
+ ALCOHOL
B = 15 kG
0.5
1.0
1.5
2.0
E (kV/cm)

FIGURE 9

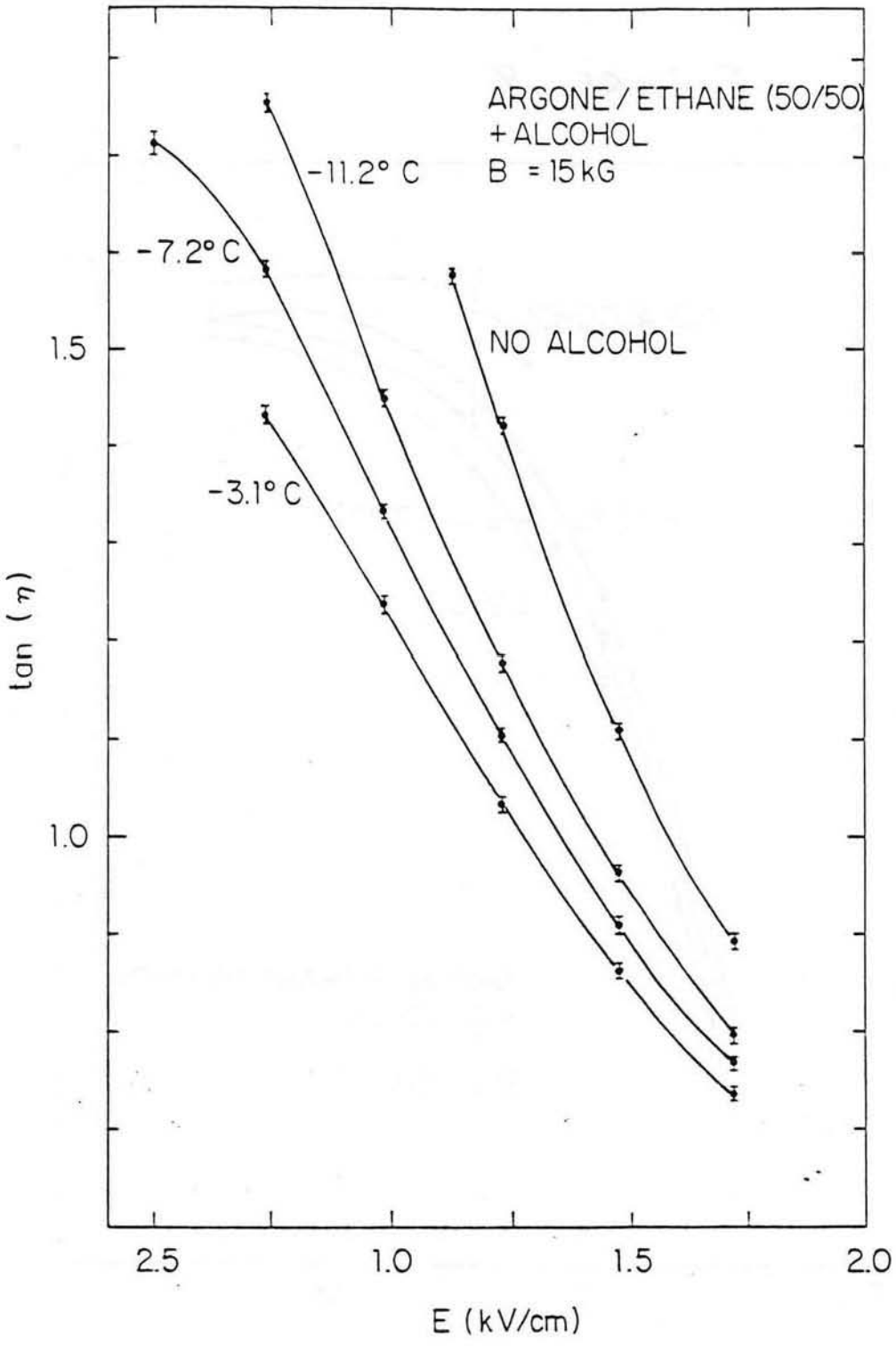
ARGONE / ETHANE (50/50)
+ ALCOHOL
B = 15 kG
-11.2° C
-7.2° C
-3.1° C
NO ALCOHOL
1.5
1.0
tan (η)
2.5
1.0
1.5
2.0
E (kV/cm)

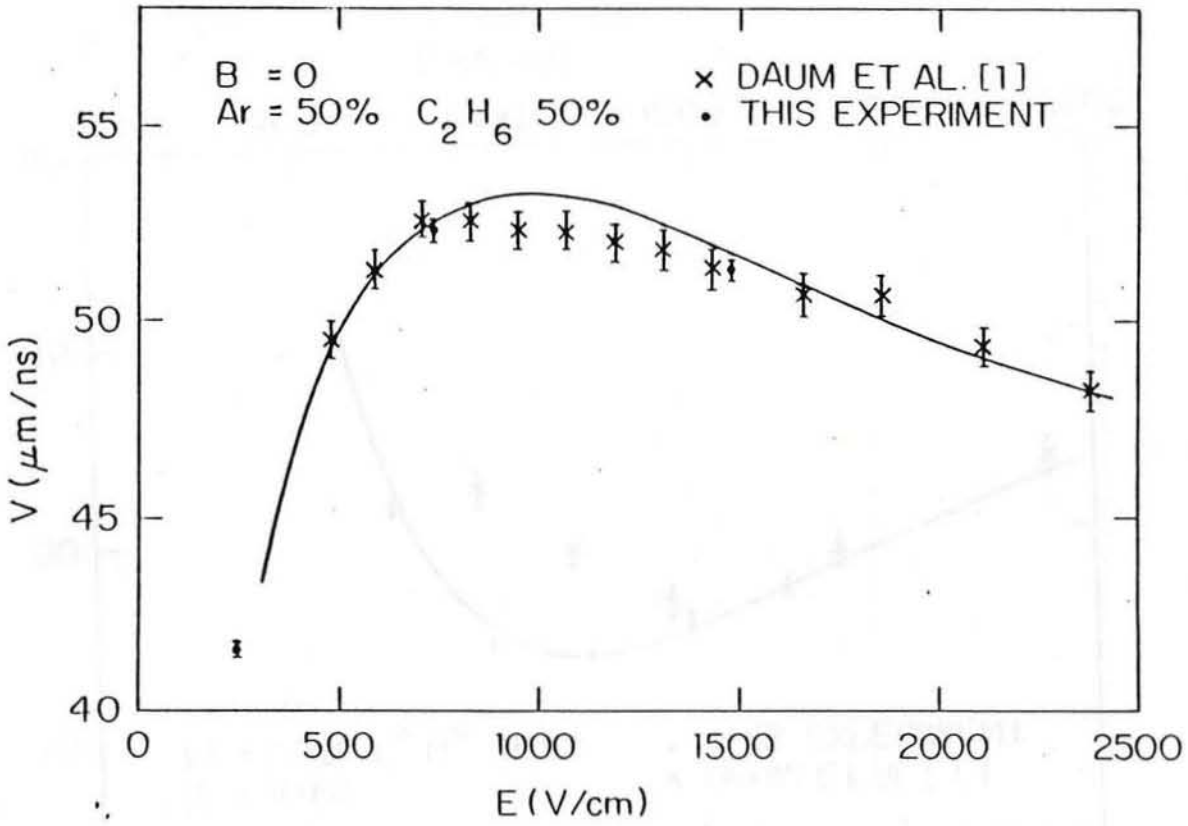
B = 0
Ar = 50% C_2H_6 50%
× DAUM ET AL. [1]
• THIS EXPERIMENT
55
50
45
40
V (μm/ns)
0
500
1000
1500
2000
2500
E (V/cm)

FIGURE 10a

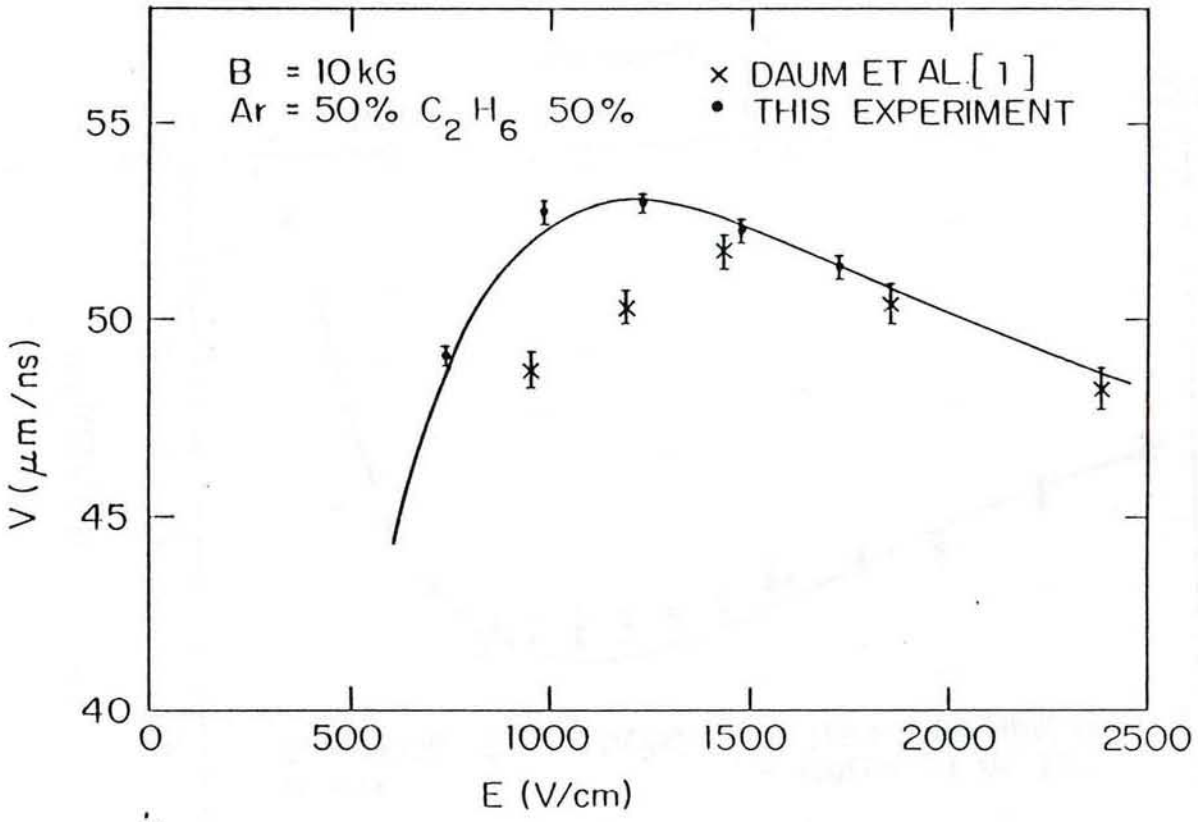
B = 10 kG
Ar = 50% C_2H_6 50%
× DAUM ET AL. [1]
• THIS EXPERIMENT
55
50
45
40
V (μm/ns)
0
500
1000
1500
2000
2500
E (V/cm)

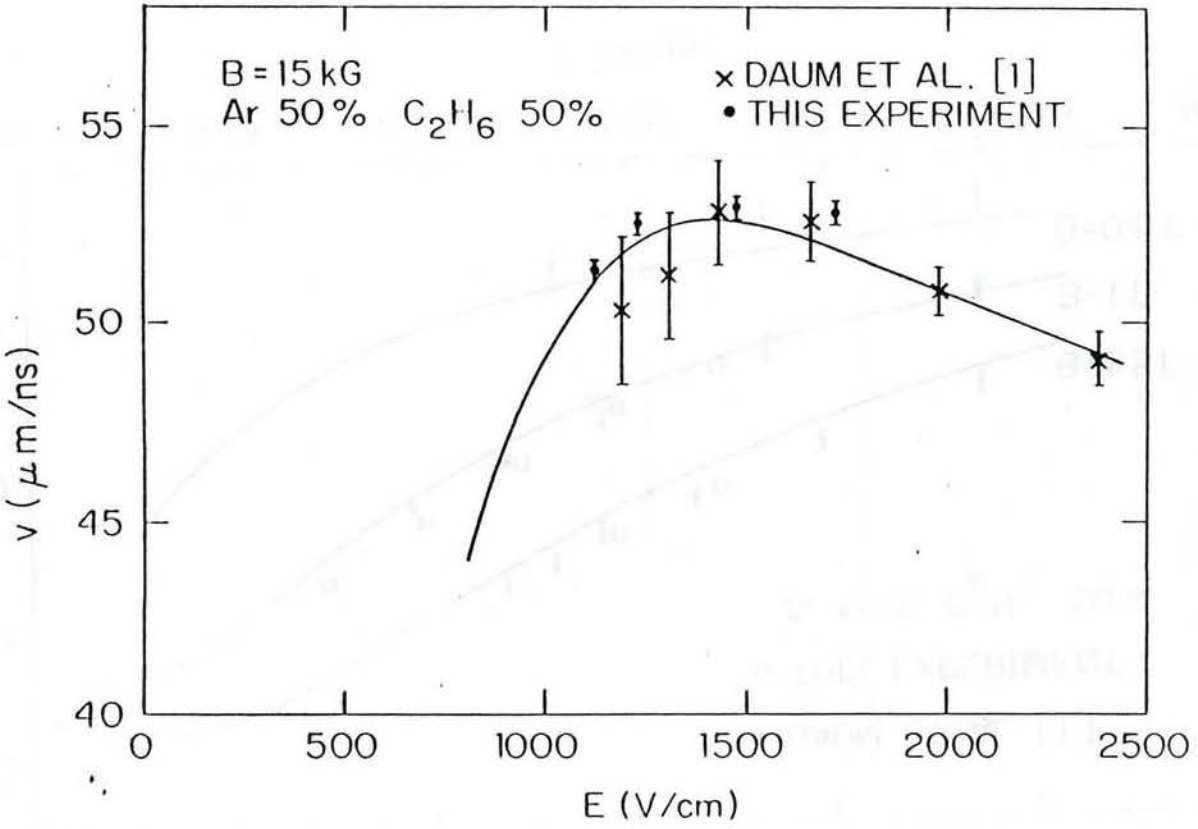
B = 15 kG
Ar 50 % C_2H_6 50%
× DAUM ET AL. [1]
• THIS EXPERIMENT
55
50
45
40
v (μm/ns)
0
500
1000
1500
2000
2500
E (V/cm)

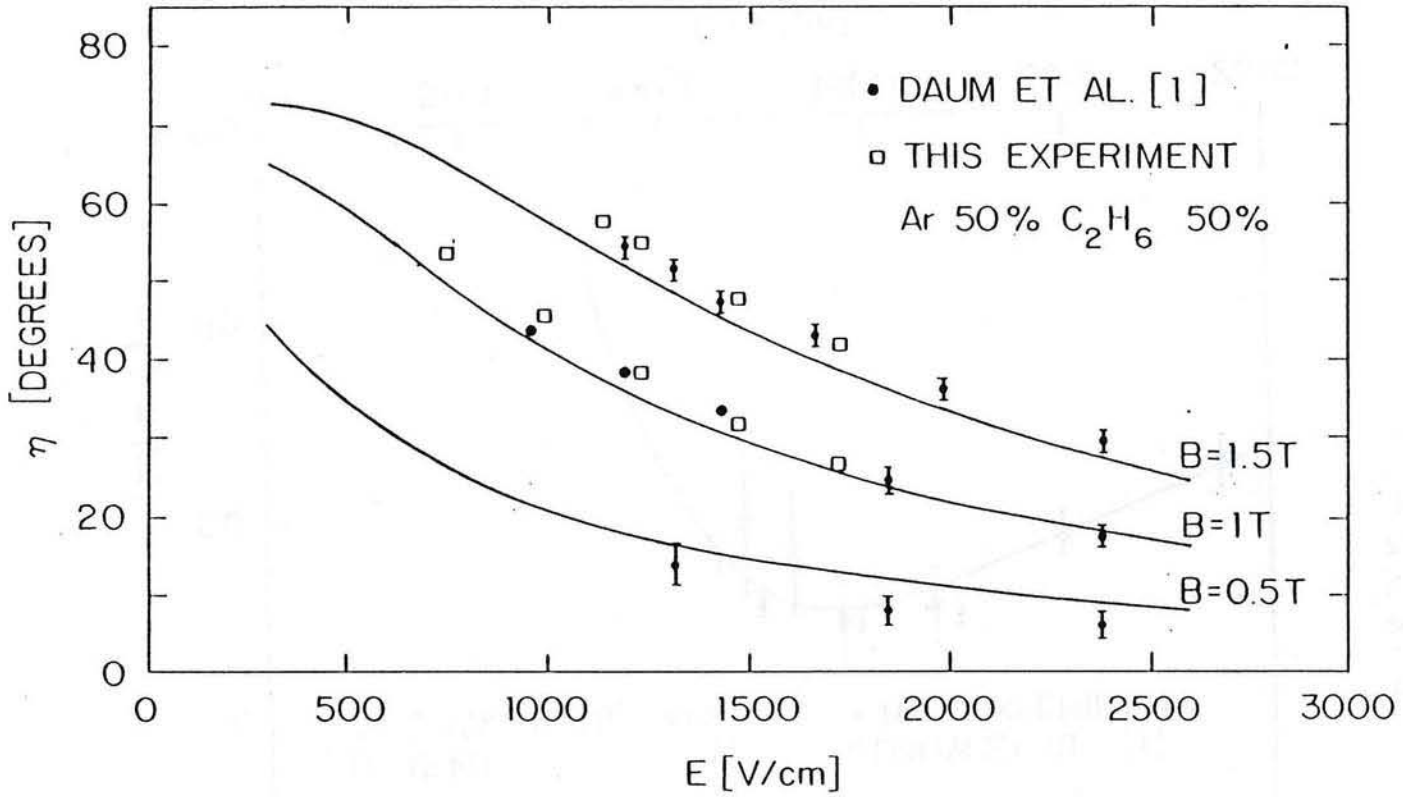
80
60
40
20
0
η [DEGREES]
0
500
1000
1500
2000
2500
3000
E [V/cm]
• DAUM ET AL. [1]
□ THIS EXPERIMENT
Ar 50% C2H6 50%
B=1.5T
B=1T
B=0.5T

Fig. 11